

An experimental investigation into the dynamics of a string

Timothy C. Molteno

Department of Physics, University of Otago, Dunedin, New Zealand

Nicholas B. Tufillaro^{a)}

P.O. Box 60276, Palo Alto, California 94306-0276

(Received 9 July 2002; accepted 30 April 2004)

We describe a detailed experimental investigation into the dynamics of a sinusoidally forced string. We find qualitative agreement with the predictions of the averaged equations of motion for a string in the high damping regime. At low damping we observe more complex phenomena not present in the averaged equations. © 2004 American Association of Physics Teachers.

[DOI: 10.1119/1.1764557]

I. INTRODUCTION

Analysis of the motions of strings has motivated a surprising amount of science: From ancient Greeks investigating the length ratios which produce harmonious sounds, to d'Alembert who developed the theory of partial differential equations in order to model the motions of a string.¹ Our reasons for studying the motions of a string are captured well by the words of P.M. Morse² who wrote in 1936: "The string is the simplest case of a system with an infinite number of allowed frequencies, and it is best to discuss some of the properties common to all such systems for as simple as a system as we can find, lest the mathematical complications completely obscure the physical ideas." More recent theoretical and numerical investigations³⁻⁸ have predicted a wide variety of nonlinear phenomena in the motion of a sinusoidally forced stretched string: for example, torus-doubling bifurcations, boundary crises, and chaos. In this paper we describe an experiment which attempts a more extensive investigation than earlier efforts to look for chaotic motions^{7,9-11} and related nonlinear phenomena in the vibration of strings and verifies, in the most part, these predictions.

We previously reported a simple exploratory experiment which established the existence of chaotic motions in strings.⁹ This previous experiment successfully observed the torus-doubling transition to chaos, but lacked the control and precision necessary for a thorough investigation of the dynamics of a sinusoidally forced string.

A more comprehensive experimental apparatus was designed for this second more detailed study. This was prompted both by a desire to improve the initial string experiment, and by further theoretical work, particularly that of Bajaj and Johnson,^{5,6} which indicated that several other interesting nonlinear phenomena, such as boundary crises, should occur in the string system.

This paper describes the results of this second investigation into a string's dynamics and is organized as follows. In order to make this paper self-contained, Sec. II outlines the derivation of the averaged equations of motion used to model the dynamics of a string and provides an extensive overview of the nonlinear phenomena predicted by these equations. Section III and the Appendix describes the experimental apparatus. Section IV presents the results of our experimental investigation.

It is hoped that some of these results could be incorporated into standard mechanics courses that touch on the linear and nonlinear motions of a string, as well as theoretical and ex-

perimental courses that are specifically focused on the study of nonlinear dynamics.¹²⁻¹⁷ For a basic background on some of the concepts and terms used in nonlinear dynamics and this paper—such as Hopf bifurcation, Logistic map, or Lorenz attractor, and so on—see an introductory text such as the book by Strogatz.¹³

II. MODELS OF STRINGS

We consider a string stretched between two fixed mounts. When the string vibrates transverse to its resting configuration, its length must also fluctuate. This coupling between the transverse motions and the longitudinal motions is nonlinear, even for small oscillation amplitudes. The simplest interesting model of a vibrating string, which takes account of this effect and allows for motion in only one transverse direction, yields a forced damped Duffing equation.¹⁸

This section starts with the full equations of motion for a forced, damped, taut string. Then, following the work of Bajaj and Johnson,^{5,6} these equations are reduced to the fundamental mode, but also allow motion in two transverse directions. Using averaging theory this results in four simultaneous ordinary differential equations, which we call the averaged equations of motion. These equations are the basis for the predictions of basic nonlinear behavior and chaos which we search for experimentally.

A. Narasimha's equations of motion

The nonlinear equations of motion governing the behavior of a string date back at least to Kirchhoff (1883).^{7,8} In this section these equations are presented as derived by Narasimha¹⁸ and the assumptions implicit in them are summarized.

Narasimha models the string as a long thin circular cylinder composed of a linear elastic solid under tension T_0 , and subject to an external forcing $\mathbf{f}(x,t)$ transverse to the resting axis. The exact equations of motion for the transverse (\mathbf{v}) and longitudinal (u) amplitudes of oscillation of such a string are, in units of the length of the string (l), mass per unit length (m_0), and velocity of propagation of transverse waves ($\sqrt{T_0/m_0}$)

$$\left(1 - \frac{\partial u}{\partial x}\right) \ddot{u} = c_1^2 \frac{\partial \Lambda}{\partial x}, \quad (1)$$

$$\left(1 - \frac{\partial u}{\partial x}\right) \ddot{\mathbf{v}} = c_1^2 \frac{\partial}{\partial x} \left(\frac{\partial \mathbf{v}}{\partial x} \Lambda \right) + \mathbf{f}(x, t), \quad (2)$$

where

$$\Lambda = \frac{1 + c_1^2 \lambda - c_2^2 \lambda^2 + c_3^3 \lambda^3}{c_1^2 (1 + \lambda) \left(1 - \frac{\partial u}{\partial x}\right)}, \quad (3)$$

$$\lambda = \left(1 + \left(\frac{\partial \mathbf{v}}{\partial x}\right)^2\right)^{1/2} \left(1 - \frac{\partial u}{\partial x}\right)^{-1} - 1. \quad (4)$$

Now Narasimha performs a perturbation analysis by expanding the apparent strain λ to

$$\lambda = \frac{\partial u}{\partial x} + \frac{1}{2} \left(\frac{\partial \mathbf{v}}{\partial x}\right)^2 + \left(\frac{\partial u}{\partial x}\right)^2 - \frac{1}{8} \left(\frac{\partial \mathbf{v}}{\partial x}\right)^2 \left(\left(\frac{\partial \mathbf{v}}{\partial x}\right)^2 - 4 \frac{\partial u}{\partial x}\right) + \dots \quad (5)$$

If we assume that the oscillation amplitudes (u and \mathbf{v}) are small, then we can approximate λ as

$$\lambda \approx \frac{\partial u}{\partial x} + \frac{1}{2} \left(\frac{\partial \mathbf{v}}{\partial x}\right)^2. \quad (6)$$

If we approximate the apparent strain as $\lambda \approx \partial u / \partial x$, then the transverse and longitudinal motions of the string are uncoupled and the transverse amplitudes (\mathbf{v}) obey a linear wave equation. The approximation in Eq. (6) is then the lowest order inclusion of the longitudinal coupling to the transverse motions.

A simple geometric argument leads to the conclusion that for small transverse amplitudes, $|\mathbf{v}| \sim \delta$, the longitudinal amplitude is $u \sim \delta^2$. For forced motions of the string we use the amplitude of forcing ϵ as a small parameter, $\mathbf{f} = \epsilon f_0(x, t)$. Expanding the longitudinal amplitude u , and the transverse amplitude \mathbf{v} , in ϵ we get

$$\mathbf{v} = \epsilon(\mathbf{v}_0 + \epsilon^2 \mathbf{v}_1 + \epsilon^4 \mathbf{v}_2 + \dots), \quad (7)$$

$$u = \epsilon^2(u_0 + \epsilon^2 u_1 + \epsilon^4 u_2 + \dots). \quad (8)$$

The equation for the transverse motions is found by neglecting all but the lowest powers of ϵ , and adding a phenomenological damping term β . The damping is assumed *a priori* to be linearly related to the velocity, and is designed to model the complex loss mechanisms such as air resistance, internal friction, and movements of the endpoints. This yields the equation of motion

$$\ddot{\mathbf{v}}_0 + \beta \omega_0 \dot{\mathbf{v}}_0 - \frac{d^2 \mathbf{v}_0}{dx^2} \left[1 + \frac{c_1^2}{2} \int_0^1 \left|\frac{d\mathbf{v}_0}{dx}\right|^2 dx\right] = \mathbf{f}_0(x, t). \quad (9)$$

In standard units, the equations of motion for the transverse amplitudes $\mathbf{r}(x, t)$ are

$$\ddot{\mathbf{r}} + 2\beta\omega_0 \dot{\mathbf{r}} - \frac{d^2 \mathbf{r}}{dx^2} \left[c_0^2 + \frac{c_1^2}{2l} \int_0^l \left|\frac{d\mathbf{r}}{dx}\right|^2 dx\right] = \frac{1}{m} \mathbf{f}(x, t), \quad (10)$$

where β is the damping on the fundamental mode, ω_0 is the fundamental frequency of transverse vibration, c_0 is the transverse wave speed, c_1 the longitudinal wave speed, m is the mass per unit length, and $\mathbf{f}(x, t)$ is the external forcing per unit length.

If we expand the transverse amplitudes $\mathbf{r}(x, t)$ and the forcing $\mathbf{f}(x, t)$ in a Fourier series,⁵ then the boundary conditions force the cosine terms to be zero and we get

$$\mathbf{r}(x, t) = \sum_{n=1}^{\infty} \mathbf{r}_n(t) \sin \frac{n\pi x}{l}, \quad (11)$$

$$\mathbf{f}(x, t) = \sum_{n=1}^{\infty} \mathbf{f}_n(t) \sin \frac{n\pi x}{l}. \quad (12)$$

Substituting into the equations of motion [Eq. (10)] we get an equation for the n th mode

$$\ddot{\mathbf{r}}_n + 2\beta\omega_0 \dot{\mathbf{r}}_n + \omega_n^2 \mathbf{r}_n \left[1 + \frac{1}{4s} \sum_{j=1}^{\infty} \left|\frac{j\mathbf{r}_j \pi}{l}\right|^2\right] = \frac{1}{m} \mathbf{f}_n(x, t), \quad (13)$$

where $\omega_n = n\omega_0$ and $s = (c_0/c_1)^2$.

Now if we assume that the external forcing is along the y axis, excites only the fundamental mode $f(t) = \mathbf{f}_1(t) \cdot \mathbf{e}_y$, and restricts $\mathbf{r}(x, t)$ to lie only along the y axis

$$\left(\mathbf{e}_y = \begin{pmatrix} 1 \\ 0 \end{pmatrix}\right),$$

i.e., let $r = \mathbf{r}_1$, then Eq. (13) becomes

$$\ddot{r} + 2\beta\omega_0 \dot{r} + \omega_0^2 r [1 + \xi r^2] = \frac{1}{m} f(t), \quad (14)$$

where $\xi = \pi^2/4sl^2$. This is a forced damped Duffing's equation governing motion confined to one transverse direction.⁴

B. Averaged equations of motion

Next we turn our attention to getting modal equations that take into account possible motions in both transverse directions. The equations of motion for the transverse amplitudes of the string [Eq. (10)], take into account the coupling between the longitudinal motions of the string and its transverse motions. Keeping only the lowest order nonlinear terms, Miles,¹⁹ and Bajaj and Johnson^{5,6} reduce these equations to a set of four ordinary differential equations for the amplitudes of the motion averaged over the fast oscillations. This section follows their derivation of these averaged equations of motion.

We start with the modal expansion of Narasimha's equation of motion [Eq. (13)], and assume that the forcing is in the vertical plane only and sinusoidal with frequency ω close to the fundamental frequency ω_1 . We write it as (using a scaling chosen with the benefit of hindsight)

$$\mathbf{f}_1 = \frac{\epsilon m l \omega_1^2}{\pi} \cos \omega t \mathbf{e}_y, \quad (15)$$

where ϵ is an amplitude of excitation and will be considered "small." We assume that the forcing frequency excites only the fundamental mode, and that the higher order modes are excited only through their nonlinear coupling to the fundamental mode. The N mode truncation of the modal equations can now be written, explicitly including a "smallness" parameter $\hat{\epsilon}$, as

$$\begin{aligned} \mathbf{z}_n'' + n^2 \mathbf{z}_n &= \hat{\epsilon} \left[2n \cos \tau_1 \mathbf{e}_y - 2\alpha \mathbf{z}_n' - 2\beta \mathbf{z}_n'' - 4n^2 \sum_{j=1}^N j^{-1} |z_j|^2 \mathbf{z}_n \right], \end{aligned} \quad (16)$$

where ' represents differentiation with respect to the timescale $\tau_1 = \omega t$ and

$$\mathbf{z}_n = \frac{\mathbf{r}_n \pi n^{3/2}}{2l(\epsilon s)^{1/3}}, \quad (17)$$

$$\alpha = 4\delta \left(\frac{s}{\epsilon^2} \right)^{1/3} \frac{\omega}{\omega_1}, \quad (18)$$

$$\beta = 2 \left(\frac{s}{\epsilon^2} \right)^{1/3} \left[\left(\frac{\omega}{\omega_1} \right)^2 - 1 \right], \quad (19)$$

$$\hat{\epsilon} = \frac{1}{4} \left(\frac{\epsilon^2}{s} \right)^{1/3}. \quad (20)$$

The dimensionless parameters α and β represent damping and detuning from the natural frequency of the fundamental mode. Bajaj and Johnson⁶ show that the energy of the unforced modes (to $O(\hat{\epsilon})$) decay exponentially to zero. This justifies taking a single mode truncation of these modal equations which gives us the equations of motion

$$\mathbf{z}'' + \mathbf{z} = \hat{\epsilon} [\cos \tau_1 \mathbf{e}_y - 2\alpha \mathbf{z}' - 2\beta \mathbf{z}'' - 4|z|^2 \mathbf{z}]. \quad (21)$$

While it is possible to directly solve this truncated modal equation numerically, averaging over the fast oscillations of the string produces a model which is more easily analyzed. Bajaj and Johnson⁶ show that, in most of the parameter regimes of interest here, predictions from the averaged equations are in close agreement with direct numerical solutions. Our experiment described in Sec. III will hopefully shed some light on the behavior of an averaged quantity, in those regions of parameter space where the averaging assumptions are violated.

Before we apply the method of averaging it is convenient to express the equations of motion as a system of first order ordinary differential equations

$$\mathbf{x}' = \mathbf{y}, \quad (22)$$

$$\mathbf{y}' = \frac{1}{1+2\beta\hat{\epsilon}} [-\mathbf{x} + \hat{\epsilon}(2 \cos \tau_1 \mathbf{e}_y - 2\alpha \mathbf{y} - 4|\mathbf{x}|^2 \mathbf{x})]. \quad (23)$$

Note that as \mathbf{x}, \mathbf{y} are two-dimensional vectors, this is a system of four coupled ordinary differential equations.

The system of equations [Eqs. (22) and (23)] is transformed into a form suitable for application of the method of averaging by the invertible van der Pol transformation²⁰

$$\begin{pmatrix} \hat{\mathbf{p}} \\ \hat{\mathbf{q}} \end{pmatrix} = A \begin{pmatrix} \mathbf{x} \\ \mathbf{y} \end{pmatrix}, \quad (24)$$

where

$$A = \begin{pmatrix} \cos \tau_1 & -\sin \tau_1 \\ \sin \tau_1 & \cos \tau_1 \end{pmatrix}, \quad (25)$$

$$A^{-1} = \begin{pmatrix} \cos \tau_1 & \sin \tau_1 \\ -\sin \tau_1 & \cos \tau_1 \end{pmatrix}, \quad (26)$$

$$A' = \begin{pmatrix} -\sin \tau_1 & -\cos \tau_1 \\ \cos \tau_1 & -\sin \tau_1 \end{pmatrix}. \quad (27)$$

Therefore we can transform the equations of motion [Eqs. (22) and (23)] to

$$\begin{pmatrix} \hat{\mathbf{p}}' \\ \hat{\mathbf{q}}' \end{pmatrix} = A' \begin{pmatrix} \mathbf{x} \\ \mathbf{y} \end{pmatrix} + A \begin{pmatrix} \mathbf{x}' \\ \mathbf{y}' \end{pmatrix}, \quad (28)$$

which, substituting for A , A' , and \mathbf{x}' from Eq. (22), is equivalent to

$$\hat{\mathbf{p}}' = -(\mathbf{x} + \mathbf{y}') \sin \tau_1, \quad (29)$$

$$\hat{\mathbf{q}}' = (\mathbf{x} + \mathbf{y}') \cos \tau_1. \quad (30)$$

Now substituting for \mathbf{y}' in terms of \mathbf{x} and \mathbf{y} [Eq. (23)] and then for \mathbf{x}, \mathbf{y} in terms of $\hat{\mathbf{p}}$ and $\hat{\mathbf{q}}$ using Eq. (24), we get

$$\begin{aligned} \hat{\mathbf{p}}' (1 + 2\beta\hat{\epsilon}) &= -\hat{\epsilon} [(\hat{\mathbf{p}} \cos \tau_1 + \hat{\mathbf{q}} \sin \tau_1)(2\beta \\ &\quad - 4(p^2 \cos^2 \tau_1 + q^2 \sin^2 \tau_1 + \hat{\mathbf{p}} \cdot \hat{\mathbf{q}} \sin \tau_1)) \\ &\quad + 2\alpha(\hat{\mathbf{p}} \sin \tau_1 - \hat{\mathbf{q}} \cos \tau_1) \\ &\quad + 2 \cos \tau_1 \mathbf{e}_y] \sin \tau_1, \end{aligned} \quad (31)$$

$$\begin{aligned} \hat{\mathbf{q}}' (1 + 2\beta\hat{\epsilon}) &= +\hat{\epsilon} [(\hat{\mathbf{p}} \cos \tau_1 + \hat{\mathbf{q}} \sin \tau_1)(2\beta \\ &\quad - 4(p^2 \cos^2 \tau_1 + q^2 \sin^2 \tau_1 + \hat{\mathbf{p}} \cdot \hat{\mathbf{q}} \sin \tau_1)) \\ &\quad + 2\alpha(\hat{\mathbf{p}} \sin \tau_1 - \hat{\mathbf{q}} \cos \tau_1) \\ &\quad + 2 \cos \tau_1 \mathbf{e}_y] \cos \tau_1. \end{aligned} \quad (32)$$

We now have the equations of motion in a "standard form" suitable for the application of averaging techniques

$$\hat{\mathbf{p}}' = \hat{\epsilon} \mathbf{g}_1(\hat{\mathbf{p}}, \hat{\mathbf{q}}, \tau_1, \hat{\epsilon}), \quad (33)$$

$$\hat{\mathbf{q}}' = \hat{\epsilon} \mathbf{g}_2(\hat{\mathbf{p}}, \hat{\mathbf{q}}, \tau_1, \hat{\epsilon}), \quad (34)$$

where the functions \mathbf{g}_1 and \mathbf{g}_2 are periodic (period 2π) in τ_1 . The associated autonomous averaged system is defined (see, for example, Guckenheimer and Holmes²⁰) as

$$\mathbf{p}' = \hat{\epsilon} \frac{1}{2\pi} \int_0^{2\pi} \mathbf{g}_1(\hat{\mathbf{p}}, \hat{\mathbf{q}}, \tau_1, 0) d\tau_1 + O(\hat{\epsilon}^2), \quad (35)$$

$$\mathbf{q}' = \hat{\epsilon} \frac{1}{2\pi} \int_0^{2\pi} \mathbf{g}_2(\hat{\mathbf{p}}, \hat{\mathbf{q}}, \tau_1, 0) d\tau_1 + O(\hat{\epsilon}^2). \quad (36)$$

Carrying out this integration we arrive at the *averaged equations of motion*

$$p_1' = -\alpha p_1 - (\beta - 1.5E)q_1 + M p_2, \quad (37)$$

$$p_2' = -\alpha p_2 - (\beta - 1.5E)q_2 - M p_1, \quad (38)$$

$$q_1' = -\alpha q_1 + (\beta - 1.5E)p_1 + M q_2 + 1, \quad (39)$$

$$q_2' = -\alpha q_2 + (\beta - 1.5E)p_2 - M q_1, \quad (40)$$

where

$$E = p_1^2 + p_2^2 + q_1^2 + q_2^2 \quad (41)$$

and

$$M = p_1 q_2 - p_2 q_1. \quad (42)$$

These equations are identical to those obtained by Miles,¹⁹ who used the method of multiple time scales. The components p_1 and q_1 are slowly varying averaged amplitudes called the *planar* components of motion because they lie in the plane of forcing. The variables p_2 and q_2 are called the *nonplanar* components. Both represent motion in the

“modulated” frequency well below the “carrier” frequency set by the forcing frequency.

The averaging theorem states that for $\hat{\epsilon}$ small enough the following results hold between the original and averaged systems: If there is a hyperbolic fixed point of the averaged system, then the original system possesses a unique hyperbolic periodic orbit of the same stability type, and that periodic solutions of the averaged equations correspond to quasiperiodic solutions of the original system of equations. In particular if a Hopf or saddle-node bifurcation occurs in the averaged system, then the Poincaré map of the original system also undergoes a Hopf or saddle-node bifurcation. Additionally, if the averaged system has a hyperbolic periodic orbit γ , then the Poincaré map has an invariant closed curve near γ and the original system has a hyperbolic invariant torus.

There are no results at present which make a formal connection between chaotic solutions of the averaged equations and the original system. Additionally the above statements only apply for sufficiently small $\hat{\epsilon}$. However, extensive numerical solutions of Bajaj and Johnson between the original and averaged equations indicate that chaotic motions and related behavior also exist between both models. The next section summarizes the results of these theoretical and numerical investigations by Bajaj and Johnson^{5,6} for the solutions to the averaged equations of motion of a string.

C. Predicted string dynamics

The averaged equations of motion were investigated by Miles²⁰ and subsequently by Bajaj and Johnson.^{5,6} Miles discovered torus doubling bifurcation sequences, but none which resulted in a chaotic attractor. Johnson and Bajaj examined higher damping regimes and discovered chaotic solutions connected to a new periodic branch of solutions. This solution they termed the *Isolated Branch* since it is not connected to the *Hopf Branch* in the parameter region explored by Miles. Further exploration uncovered many interesting phenomena including the formation of a homoclinic orbit, boundary crises, and intermittency. We summarize some of the predicted results in this concluding theory section. For a more complete discussion and illustrations see the papers by Bajaj and Johnson.^{5,6}

The averaged equations of motion for the string are invariant under sign change of the nonplanar components of the motion $(p_2, q_2) \rightarrow (-p_2, -q_2)$. This means that for every solution found numerically, there is another mirror-image solution which is found by making this sign change.

We start the discussion of the dynamics generated by these equations (37)–(40) with a summary of the behavior of their fixed points which are known, from the averaging theorem,²⁰ to correspond to periodic trajectories of the unaveraged equations of motion [Eqs. (31) and (32)].

1. Fixed points

The fixed points of the averaged equations can be determined as functions of the detuning parameter β , and the damping parameter α . The plot of the amplitude of the averaged motion E , against detuning β for some fixed damping α is called a *constant amplitude response curve*. These curves are simply the familiar resonance curves, plotting amplitude of oscillation versus frequency.

The stability of the fixed points divides the motions of the string into several classes catalogued by their damping values. These are:

- $\alpha > 0.991$. All motions are confined to the plane of excitation ($p_2 = q_2 = 0$). These are the only stable constant solutions to the averaged equations in this regime, and the amplitude is a single valued function of the detuning. This is called the *planar solution branch*.
- $\alpha < 0.991$. The motions on the planar solution branch can become multivalued over some frequency intervals. Typical response curves in this regime, are confined to the plane, but in some detuning frequency intervals denoted by $\Delta\beta$ there are three possible steady state solutions. In this regime, the string exhibits hysteresis as the detuning is varied. That is constant amplitude response curves exhibit different transition jumps depending on whether the frequency scan is slowing increasing or decreasing—a so-called “upward” or “downward” scan. These transitions occur when the current planar solution branch loses stability and the motion jumps to another stable branch which are typically created via saddle-node bifurcations.
- $\alpha < 0.687$. Orbits are no longer confined to the plane of excitation. These are the so-called “whirling” motions. There are at least two non-planar whirling solutions—a clockwise and counterclockwise orbit—because of the reflection symmetry in the ($p_2 = q_2 = 0$) plane. These branches are single valued for damping values larger than $\alpha = 0.477$. The transition from planar to non-planar motion is usually quite easy to detect experimentally since the string literally “pops” out from a single plane of motion as a parameter is changed.
- $\alpha < 0.477$ The nonplanar whirling solutions can also become multivalued, so again the system can exhibit jumps between different orbits and show complex hysteresis effects as the control parameters are slowly varied.

2. Periodic solutions

The plane defined by $p_2 = q_2 = 0$, i.e., the plane of forcing, is an invariant manifold of the averaged equations for the string [Eqs. (37)–(40)]. Bendixson’s criterion for the nonexistence of limit cycles in a two-dimensional flows says that if the expression

$$\frac{\partial p'_1}{\partial p_1} + \frac{\partial q'_1}{\partial q_1}$$

is not identically zero and does not change sign, then there are no closed orbits. For motions restricted to the plane of forcing, this expression is equal to -2α and therefore there are no planar periodic solutions to the averaged equations. Any periodic solutions must arise as solutions of the complete four-dimensional equations of motion.

3. Hopf branch

Hopf bifurcations occur in the nonplanar branch for $\alpha < 0.577$. These lead to limit-cycles (they occur in pairs due to symmetry) which are stable for damping values near to 0.577. These motions are said to lie on the Hopf solution branch. As the damping is lowered below this value, the limit cycles undergo period-doubling bifurcations. Starting with the Hopf bifurcation which creates the Hopf branch, there is

a sequence of period-doubling bifurcations followed by inverse period-doubling bifurcations back to the point at which the Hopf branch disappears in an inverse Hopf bifurcation. These periodic solutions of the averaged equations of motion correspond to quasiperiodic motions of the string.

The loci in the α - β plane for the onset and disappearance of quasiperiodicity form the Hopf bifurcation set. In the experimental section we show data outlining a Hopf bifurcation set.

4. Isolated branch

While numerically investigating the Hopf solution branch, Johnson and Bajaj⁵ discovered another disconnected but coexisting solution branch. They conjectured that it arises because of a global saddle-node bifurcation which causes a stable and unstable limit-cycle to appear for low enough damping. This *isolated* solution branch possesses motions with characteristics that are qualitatively different from the Hopf branch orbits. In particular, the isolated branch orbits exhibit “sharp” points in their orbit plots, which allow them to be distinguished from the Hopf branch orbits. For low enough damping, the isolated solution branch is connected to the Hopf branch by an unstable limit-cycle. Because the isolated branch is created by a saddle-node bifurcation, we expect to see hysteresis in its connection to the Hopf branch in this regime.

5. Chaotic solutions

According to the model equations, the isolated branch undergoes a sequence of period-doubling bifurcations which eventually results in the appearance of a chaotic attractor. As the damping is reduced below the point where the isolated branch merges with the Hopf branch, a series of isolated branches are created via saddle-node bifurcations and subsequently merge with the main solution branch. This sequence of orbit creation followed by merger, followed by another creation, terminates in the formation of a homoclinic orbit. The orbit originates from a saddle-type fixed point whose eigenvalues satisfy Shilnikov’s criterion. Bajaj and Johnson conjecture that the Shilnikov mechanism²⁰ is responsible for the stretching and folding which causes the chaos. The Shilnikov mechanism involves a homoclinic orbit from a fixed point which has one real, and a complex conjugate pair of eigenvalues.²¹ If the magnitude of the real eigenvalue is larger than the real part of the complex pair, then Shilnikov showed that return maps defined near the homoclinic orbit contain horseshoes²²—stretching and folding maps which produce chaotic behavior.

For orbits near to the homoclinic orbit, there is a branch of solutions which encircle both nonplanar fixed points (again, there are two because of the symmetry under sign change $(p_2, q_2) \leftrightarrow (-p_2, -q_2)$). According to simulations, this branch undergoes a series of bifurcations which leads to the formation of Lorenz type chaotic attractors (roughly, chaotic attractors which encircle two fixed points).²²

6. Crises

For damping values below 0.495, the chaotic solutions can suddenly be destroyed by a boundary crisis.²³ The chaotic attractor comes into contact with the stable manifold of a fixed point and the chaos is extinguished. The points at which this crisis occurs move closer to the Hopf bifurcation

points as the damping is reduced further. This reduces the interval of detuning in which the interesting periodic and chaotic motions can occur. Bajaj and Johnson conclude that eventually for $\alpha=0.25$, “practically all initial conditions lead to the lower planar steady-state constant solution.”

D. Summary of predictions

The early work of Miles¹⁹ and the more recent work of Bajaj and Johnson^{5,6} provided a lot of information about interesting behavior to look for in the motions of a string. They predict that:

- For small enough damping, the nonplanar solutions become unstable and form, via a Hopf bifurcation, the Hopf branch—a branch of limit-cycle solutions (quasiperiodicity of the string’s motion). This branch exhibits period-doubling bifurcations but these do not lead to a chaotic attractor.
- At lower values of damping, there is another coexisting branch of limit-cycle solutions, the isolated branch, which is created via a saddle-node bifurcation.
- The isolated branch has a period-doubling transition to chaos which results in a Rössler type chaotic attractor.²²
- For lower damping still, a series of isolated branches appear (via saddle-node bifurcations) and merge with the Hopf branch. This sequence ends in the creation of a homoclinic orbit, whose fixed point has eigenvalues which satisfy Shilnikov’s inequality. Lorenz type chaotic attractors are found in the neighborhood of this homoclinic orbit.
- Finally as the damping is reduced yet again, the chaotic attractors are progressively destroyed by boundary crises, eventually eliminating all interesting behavior completely.

The rest of this paper describes experiments which were designed to explore these predictions.

III. EXPERIMENTAL APPARATUS

Our string experiment is constructed from a thin wire which is subject to an external periodic forcing. The wire is driven by passing a sinusoidal current through it while resting in a permanent magnetic field. The force per unit length along the wire is a product of the magnetic field strength and the current in the wire. The forcing method is used because most theoretical studies assume a constant excitation per unit length when modeling the string. A disadvantage of this forcing technique is that the string must be made of a nonmagnetic material, otherwise the motion will be confined to a plane. A magnetic material can be used when purely planar oscillations are desired. Also, because of heating in the wire, the system is prone to slow temperature drifts, which effectively cause a very slow parameter variation (drift) in the wire’s length.

Several types of wires were tested. This experimentation showed that a thoriated tungsten wire, 0.15 mm in diameter, worked well. Tungsten is nonmagnetic so the nonplanar motions are not damped. Further, under the conditions of our experiment, the wire was well within its linear elastic response regime. The nonlinear behavior observed here is thus not an effect of the material nonlinearity, but arises from the fundamental geometry of the string deformation.

The wire is mounted between two clamps, held apart by a steel frame which also forms the yoke of the forcing magnet.

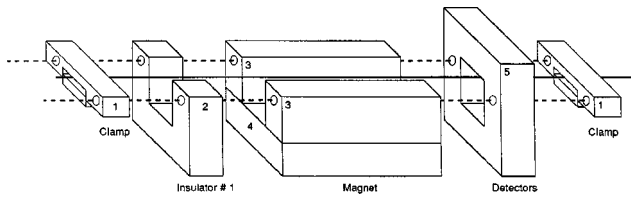


Fig. 1. Schematic of the string mounting system.

Mounted along the yoke are five pairs of rare earth ceramic (RES 190) magnets (Philips catalog No. 4313 059 6601) which provide a field of 0.2 T along the forcing length of the wire. The clamps are electrically insulated from one another by two pieces of polyvinyl chloride, one of which holds the amplitude detector. Figure 1 shows a schematic and of the mounting fixture.

The amplitude detector consists of an infrared photo diode (OP 165D) coupled to a match infrared phototransistor (OP 505D) mounted in a low- Q plastic block. Partial occlusion of the beam by the string causes the amount of light at the phototransistor to vary with the position of the string.²⁴

In addition to the rig for holding the wire, we also developed a digital electronic system for signal synthesis, processing, and visualization which is described in the Appendix and in great detail in Refs. 10 and 25. The system allows for the real-time control and real-time signal analysis of the string's vibrations. The string controller provides control over the forcing of the string as well as triggering outputs for data collection. Its basic functions are to take an input square wave and provide the following outputs:

- a forcing sine wave;
- the sampling trigger at regular intervals 32 times per forcing period; and
- a pulse once per forcing period for controlling the intensity of an oscilloscope beam (for analog Poincaré sections).¹²

We sample the motion of the string an integer number of times per forcing period. This sampling technique allows us to average the amplitude of the string over one forcing period.

The current electronics could easily be replaced with a peripheral component interconnect (PCI) plug-in board such as National Instruments PCI-6036E for signal synthesis, control, and data collection. Such a board can be programmed using MATLAB'S Data Acquisition Toolbox. For instance, we recently built such a low-cost system to do stimulus-response testing and model creation for nonlinear electronic circuits.^{26,27}

IV. EXPERIMENTAL RESULTS

The results of the string experiment are presented in order of increasing complexity: starting with simple periodic motions and ending with chaotic oscillations.

A. Periodic motion

After the constant solutions, the next simplest solutions of a sinusoidally forced pretensioned string are periodic, with period equal to the forcing signal. These periodic solutions are characterized by their rms amplitude $R_i(t)$, which is related to the slowly varying averaged amplitudes (p_i, q_i) , by

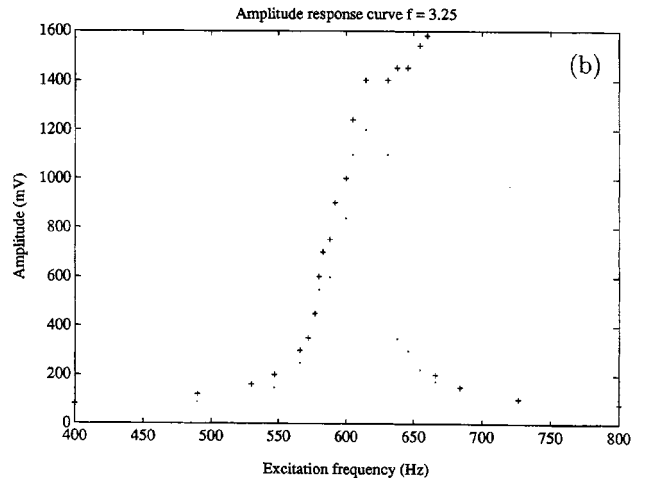
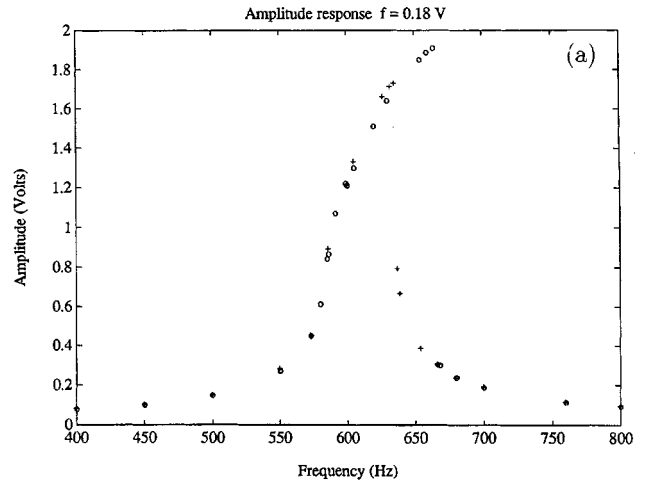


Fig. 2. Constant amplitude response curves from the string experiment: (a) before the onset of nonplanar motion and (b) after nonplanar motion. Some hysteresis is evident between the "upscans" (+) and "downscans" (o).

$$R_i(t) = \frac{1}{\sqrt{2}} \sqrt{(p_i^2 + q_i^2)} = \frac{1}{\sqrt{2}} \sqrt{E_i}. \quad (43)$$

$R_1(t)$ and $R_2(t)$ represent slowly varying amplitudes of the *planar* and *nonplanar* components of the motion, respectively. When the motions are periodic, these amplitudes are constant.

Fixing the forcing amplitude to give the desired damping (α), and then measuring the rms amplitude of the string's response for a range of forcing frequencies, gives a constant amplitude response (CAR) curve. The interesting range of forcing frequencies, for large damping, is typically less than 25 Hz on either side of the resonance (f_0). Figure 2 shows a series of experimental CAR curves which are in qualitative agreement with the predictions of the averaged models. Similar experimental results are presented by Hanson *et al.*¹¹ The damping at which the rms amplitude becomes multivalued (onset of hysteresis) provides the first quantitative test between the experiment and the averaged equations model. The model predicts that this should happen for values of $\alpha < 0.991$. In the experiment this is only observed to occur at values of $\alpha < 0.65$.

As the forcing amplitude is increased, the amplitude of the nonplanar components starts to increase and the string begins to whirl around its resting state. The onset of nonplanar motion is predicted to occur at values of $\alpha < 0.687$, and is observed experimentally at values of $\alpha < 0.45$. Notice that the ratio of the two values (experiment to theory) is approximately the same (≈ 0.65) in both instances. This might suggest that the difference may be due to errors in measuring fixed parameters of the experimental system, such as the forcing length of the string or the magnetic field strength. Alternatively, it could be that the model fails to account accurately for some basic phenomenon like damping, or that quantitative discrepancies could also arise due to some of the assumptions made in deriving the averaged model equations.

Because the model is symmetric about the vertical axis, two nonplanar (whirling) motions coexist corresponding to different directions of whirling (clockwise or counterclockwise). These two solutions can not be distinguished by their CAR curves, but can be distinguished by plotting the nonplanar average amplitudes p_2 versus q_2 . The solutions appear as fixed points in either the upper right, or lower left quadrant of the p - q plane, according to the direction of the whirling. In the experiment one of these directions is preferred, thus apparently breaking the symmetry present in the averaged equations. Whirling motions of either direction could be induced by deliberate perturbation, but left to its own devices the system would almost invariably jump to nonplanar motion in one particular direction. This asymmetry could be introduced by a nonuniformity in the silicone coating applied to the wire for damping, or by asymmetries in the clamps holding the wire.

B. Quasiperiodic motion

As the amplitude of forcing is increased, the string can jump, via a Hopf bifurcation, from periodic orbits described in the previous section to more complex motions with a periodically modulated amplitude. These quasiperiodic motions are the first step in the torus doubling route to chaos predicted by Bajaj and Johnson⁵ and described experimentally by Molteno and Tufillaro.⁹

The nonplanar periodic motions are roughly elliptical in cross section, and quasiperiodicity arises when this ellipse starts to precess. Figure 3 shows an experimental recording of the variations in the rms amplitude of a quasiperiodic signal from the string experiment. The period of the amplitude modulation in this example is approximately 250 forcing periods. Thus, the modulation frequency is slow compared to the forcing frequency. The use of averaging theory in deriving the “averaged equations of motion” would thus appear to be appropriate in this regime. Additionally, the long period of this modulation may be one reason why previous experimenters have found amplitude modulated chaotic motion difficult to observe. Most experiments have been performed on strings with a frequency of free vibration more than 1 order of magnitude lower than in this experiment (for example O’Reilly and Holmes⁷ used 88 Hz). Therefore, the modulation period is several seconds, during which time the system is susceptible to low frequency noise, which is very difficult to eliminate.

The Hopf bifurcation set is recorded by scanning the forcing frequency (changing β) for a series of different forcing amplitudes (changing α) and noting the onset and disappearance of quasiperiodicity. Figure 4 shows the experimental

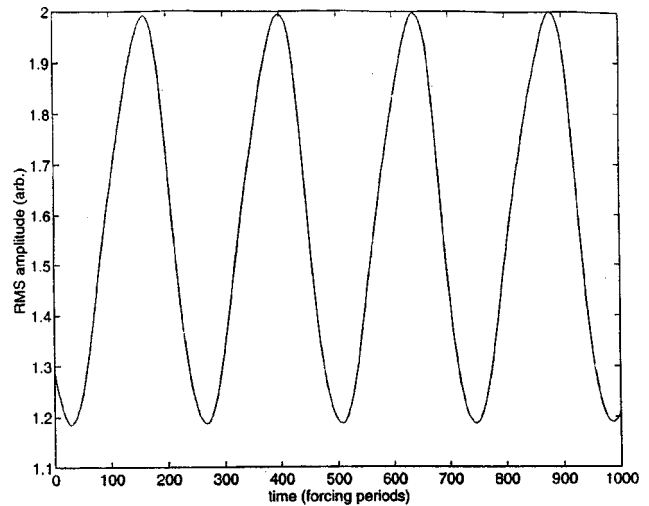


Fig. 3. A time series of the planar rms amplitude for an experimental solution after the onset of quasiperiodicity.

Hopf bifurcation set recorded from the damped string. The lower branch of the plot corresponds to creation of the Hopf branch and the upper branch corresponds to its destruction. For damping values lower than those shown on this plot, the onset of quasiperiodicity occurs at approximately the same detuning, but the Hopf branch is destroyed by an apparent crisis. The detuning at which this crisis is very sensitive to small perturbations, the Hopf branch appears to be losing stability both as the damping is lowered and as the detuning is increased.

In contrast, the upper branch of the Hopf bifurcation set predicted from the averaged equations model extends over a greater range of damping values. The bifurcation sets from the experiment and the averaged model have many features in common despite the apparent instability of the Hopf branch in the experiment, which leads to its early destruction. The critical point found experimentally for the onset of quasiperiodicity is $\alpha = 0.38, \beta = 3.4$, whereas analysis of the averaged equations yields $\alpha = 0.577, \beta = 3$. Once again, the ratio of experimental to theoretical damping for this critical point is approximately 0.65.

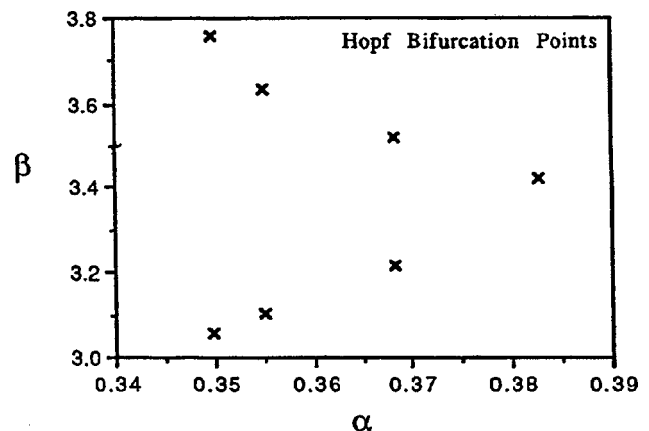


Fig. 4. The experimental Hopf bifurcation set after being transformed to the (α, β) plane.

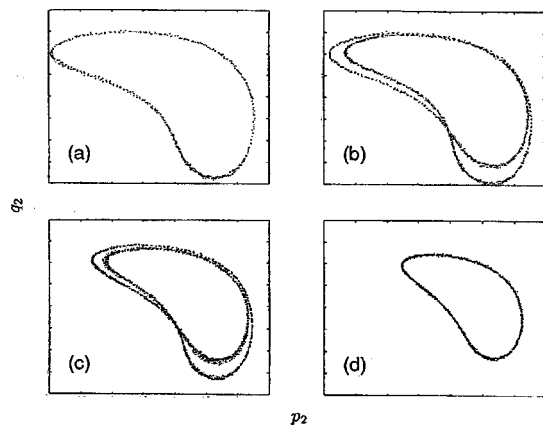


Fig. 5. A simple experimental recording of a bifurcation sequence showing a period doubling bifurcation sequence followed by an inverse period doubling bifurcation in the Hopf branch. The forcing frequency is the bifurcation parameter ($I_{\text{rms}}=0.108$ A, $f=1300$ Hz, $\alpha=0.408$).

C. Hopf branch: period doubling

For damping values just below the onset of quasiperiodic motion, the rms amplitude of the string show a period-doubling bifurcation. A typical experimental sequence of motions observed on the Hopf branch when scanning the forcing frequency is shown in Fig. 5. This contains a succession of plots of the nonplanar average amplitudes (p_2 versus q_2) which show the bifurcation sequence *period one* \rightarrow *period two* \rightarrow *period four* \rightarrow *period two* \rightarrow *period one*.

Periods larger than period four were not observed in the string experiment. This may be due to parameter drift which could obscure the observation of delicate motions on small parameter intervals, or it may reflect the actual dynamics. These period doubling bifurcations of the averaged motion correspond to torus doubling bifurcations of the amplitude of the string. This behavior is consistent with that of the Hopf solution branch of the averaged equations of motion. In this parameter regime, soon after the onset of quasiperiodicity, there seems to be excellent qualitative agreement between experiment and the averaged model.

D. Isolated branch and chaos

As the forcing amplitude increases beyond the values at which the Hopf branch appears, the string's motion can jump to a qualitatively different type of quasiperiodic solution. This jump exhibits hysteresis, i.e., the new motions persist if the forcing amplitude is reduced immediately after the jump occurs. Thus, the new motion can coexist with the Hopf branch solutions. An example of these new motions is shown

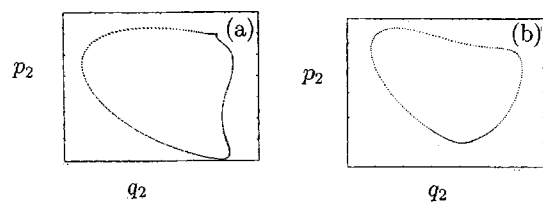


Fig. 6. Two qualitatively different quasiperiodic (period-one nonplanar rms amplitude) experimental plots. Both take with a forcing amplitude of $I_{\text{rms}}=0.110$ and at the same forcing frequency: (a) Hopf branch and (b) isolated branch.

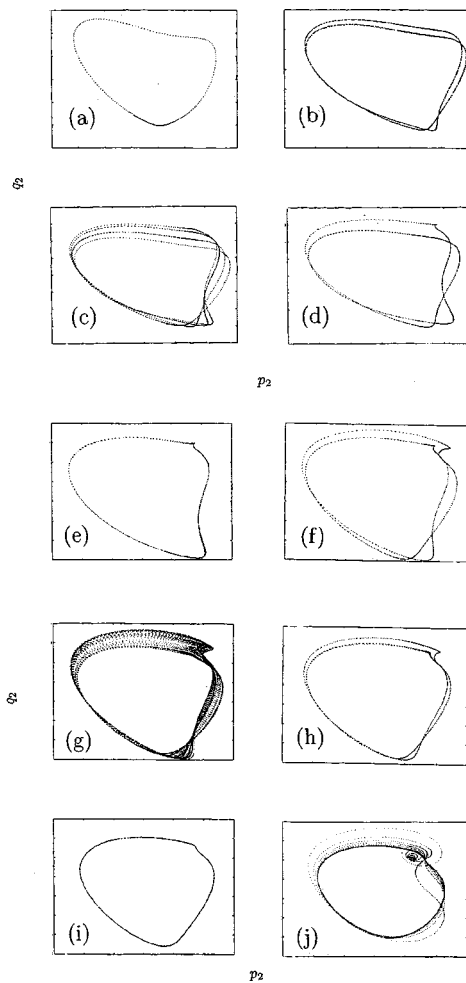


Fig. 7. A bifurcation sequence showing the merging of the Hopf branch and the isolated branch (going through chaotic motions and ending in crisis). (a) The period-one solution on the Hopf branch. (b) Period-two motion. (c) Period-four motion; these are stable over a small parameter range and can be hard to observe because of parameter drift. (d) Back to period two with no chaotic window. The period two shows "characteristics" of the isolated branch solution before it merges with the period one isolated branch orbit. (e) Period-one isolated branch orbit. (f) Period-two isolated branch orbit. (g) Chaotic isolated branch orbit. (h) Back to period-two isolated branch orbit. (i) Period-one isolated branch orbit at end of the bifurcation sequence which goes through chaos. (j) Isolated branch is destroyed by a crisis.

in Fig. 6(b) which also shows for comparison a solution from the Hopf branch [Fig. 6(a)]. The distinguishing characteristic is a peak (sharply pointed section of the trajectory) where the orbit is attracted towards the upper planar fixed point which is unstable (leading to the nonplanar solutions). All these observations are consistent with the conjecture that these new orbits correspond to the isolated branch solutions of the averaged equations.

On the isolated branch, an increase in the forcing amplitude results in a period doubling cascade (of the rms signal) which can lead to the formation of a chaotic attractor. This is demonstrated in the bifurcation sequence shown in Fig. 7 which starts on the Hopf branch, jumps to the isolated branch, and then period doubles to form a chaotic attractor. This is followed by an inverse sequence of bifurcations, which leads back to the Hopf branch. These observations are once again consistent with the predictions made from the averaged model. An interesting feature of these bifurcation

sequences is the presence of period-two solutions which share characteristics of both the Hopf branch and the isolated branch. Such solutions are not described in the simulations of Bajaj and Johnson.^{5,6} However, until an exhaustive search has been carried out, we don't know whether or not these results are consistent with the averaged model.

Some of the plots in Fig. 7 provide an example of a complex sequence of bifurcations first termed "bubbles" by Knobloch and Weiss.²⁸ They are also seen by Bajaj and Johnson in their simulations of the averaged equations. This is significant because these bubble sequences are associated with homoclinic orbits whose fixed point has eigenvalues which satisfy Shilnikov's inequality, i.e., the real eigenvalue is larger than the real part of the complex eigenvalues.²⁰ Shilnikov showed that in this circumstance there are horseshoes present in return maps defined near the homoclinic orbit. This provides anecdotal evidence that the Shilnikov mechanism is causing chaos in this parameter regime.

Figure 8(a) shows a chaotic time series from the string experiment in the p_2 - q_2 plane. The power spectrum of this time series [see Fig. 8(b)] shows the continuous structure consistent with either chaotic motion or colored noise.

1. First return map

Averaging over the fast oscillations reduces the dimension of the trajectory by one. Similarly, if a Poincaré section can be defined on this reduced trajectory then the trajectory is further reduced to the orbit of a map $x_{n+1}=f(x_n)$ and the dimension is reduced by one again. This map, f , called the *first return map*, is conveniently displayed by plotting x_n against x_{n+1} .

If we take x_n to be the n th point [measured at the intersection of the chaotic trajectory and the line indicated in Fig. 8(a)] then we get the first return map shown in Fig. 8(c). The simplicity of this map is striking and illustrates the low dimensionality of chaos in a string. It is a unimodal map very similar to the Logistic map²² (the canonical example of a simple deterministic chaotic system) and indicates that the stretching and folding of a horseshoe is causing the sensitive dependence to initial conditions in these chaotic time series. Despite the complexity of the partial differential equation model first proposed by Kirchhoff (formally an infinite-dimensional dynamical system), our study provides direct evidence that for some parameter regions the chaotic motions of a string can be modeled by a simple unimodal map (a one-dimensional dynamical system). This conclusion is supported by dimension calculations using a box-counting algorithm²⁹ which indicates that the dimension of the original attractor is about 2.3, as well as by a more sophisticated "topological" analysis of these data sets.²²

2. Banded chaos

Not all the chaotic time series in this parameter regime show a continuous unimodal first return map. In most instances, if the attractor appears soon after a period-two limit cycle, then the period-two solution seems to dominate the chaos and the strange attractor looks like a band about the period-two orbit [see Fig. 9(a)]. The unstable period-one solutions are not in the closure of the invariant set formed by the chaotic attractor. This appearance of a banded chaotic attractor, which is dominated by the period two orbit is similar to that seen in the numerical solutions of the averaged equations of Miles for spherical pendulum.³⁰

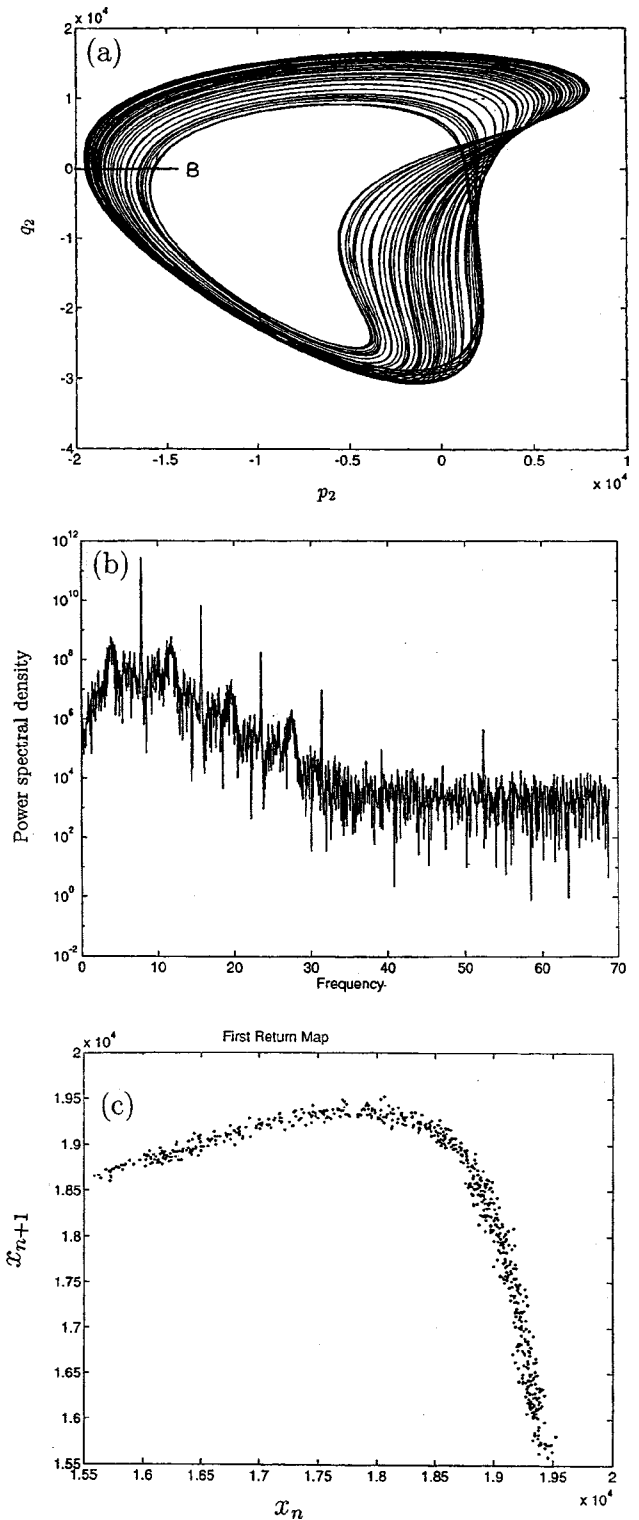


Fig. 8. Experimental chaotic time series $I_{\text{rms}}=0.11$, $f_0=1.38$ kHz. (a) Each point represents the p_2 , q_2 variables sampled once per forcing period. The return time for this time series is approximately 250 forcing periods. (b) The power spectrum. (c) The first return map at the Poincaré section. The x_i values are the intersection of the chaotic trajectory at the line shown in (a).

During the transition to chaotic behavior, the doubled torus usually breaks into a chaotic band in the immediate neighborhood of the torus. We call this *banded chaos*. The chaotic bands then become wider until they finally join and

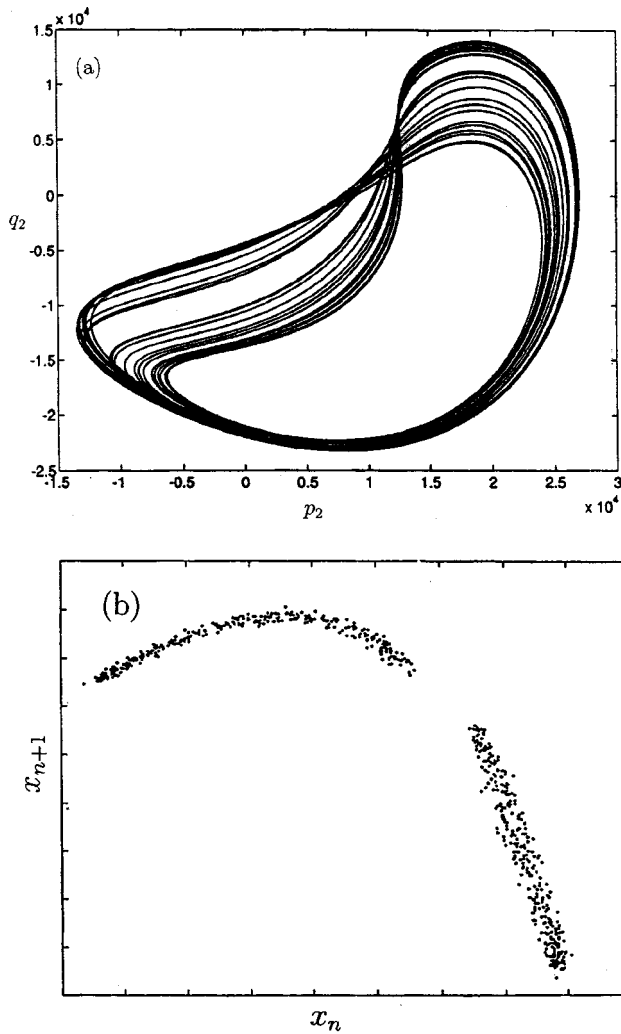


Fig. 9. Chaotic orbit showing “banded” chaos. (a) Chaotic time series soon after the period-two limit cycle. (b) First return map showing the absence of a period-one orbit resulting in a “banded” structure.

occupy the neighborhood of the period one orbit (undoubled torus). This sequence of motions is seen in both simulations of the model equations and the experiment.

E. Crisis

As the forcing amplitude is increased beyond the point of onset of chaos in the isolated branch, the chaotic attractor can suddenly be destroyed by a boundary crisis.^{23,31} This is perhaps not surprising as Grebogi *et al.*²³ show that these crises are common in systems which are close to unimodal maps. Figure 10 shows a time delay embedded experimental time series of the planar rms amplitude before and after the crisis point.

F. Intermittency

Transitions to intermittent chaos are seen in the string experiment. The intermittency transition to chaos begins with a periodic state, then burst to an intermittent state as a parameter is increased above a critical value. These bursts appear at seemingly random times, but become frequent as a control parameter is increased. Figure 11 shows an experimental time series during which bursts are occurring at a relatively

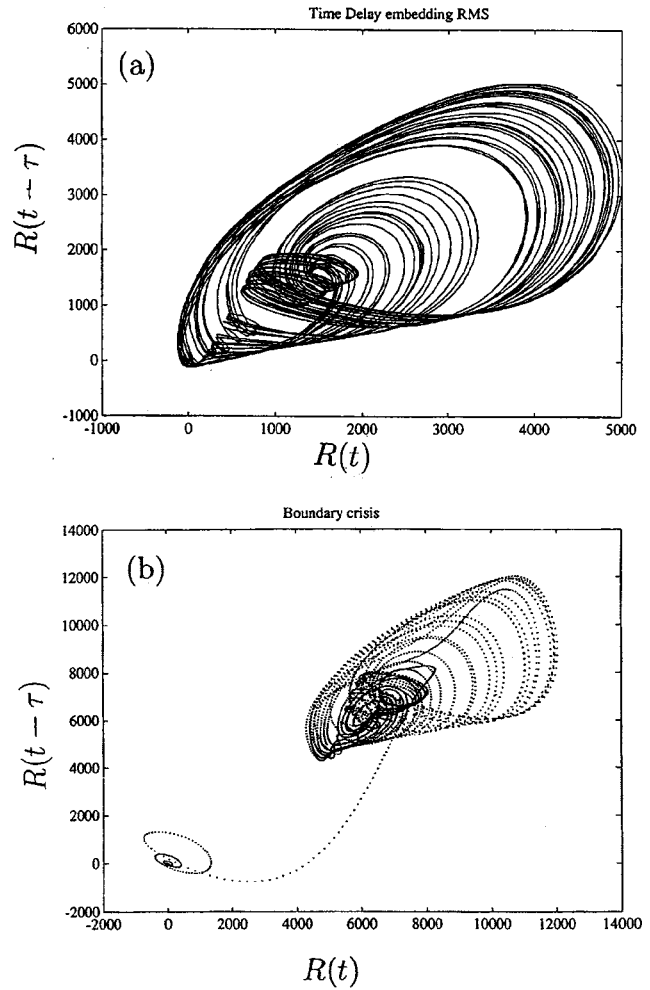


Fig. 10. Boundary crisis: (a) nonplanar rms amplitude (in arbitrary units) plot just before a boundary crisis and (b) after boundary crisis, the “ghost” of the strange attractor in (a) is clearly visible.

high rate. This figure is one of the more complex types of behavior which are observed at low damping. This intermittent behavior does not seem to be predicted by the equations for the averaged model.

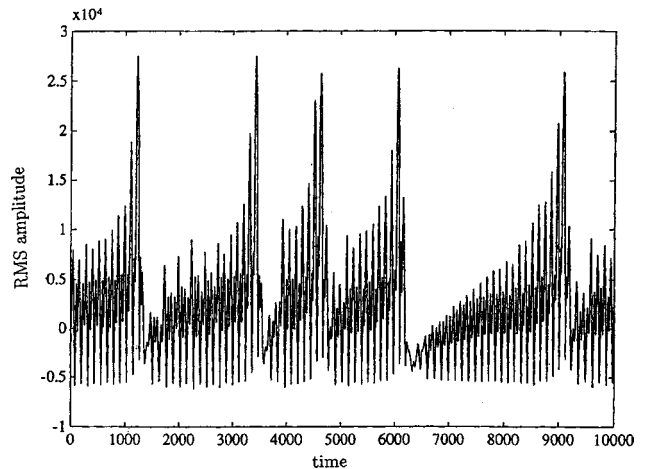


Fig. 11. Intermittency of the nonplanar rms amplitude, $I_{rms} = 28$ mA, $\alpha = 0.1$. Time is in units of forcing periods.

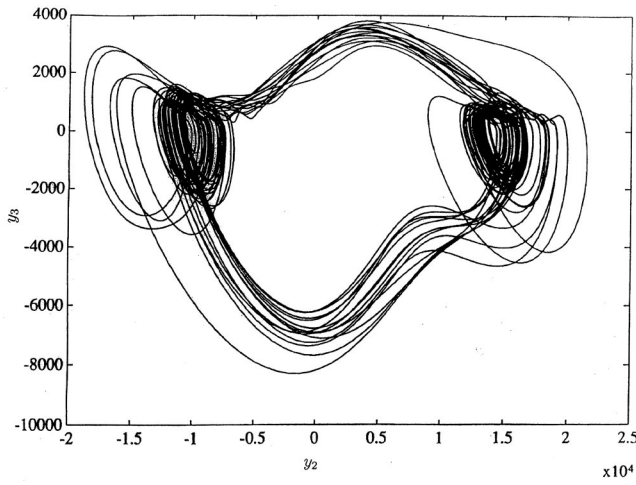


Fig. 12. Lorenz like chaotic attractor in the non-planar component of motion for $\alpha=0.1$. This data have been embedded from a single nonplanar time series using the differential-integral embedding.

G. Very low damping

Bajaj and Johnson conclude, from their observations of the behavior of the averaged equations of motion, that for damping values smaller than $\alpha=0.25$ all the interesting motions of the string system are destroyed by boundary crises: “... as the damping is lowered, the frequency over which the non-planar complex motions exist decrease, so much so that, for $\alpha=0.25$ the critical frequencies at which crisis occurs essentially coincide with β_1^* and β_2^* and practically all initial conditions lead to the lower planar steady-state constant solution.” In the above quote β_1^* and β_2^* are the Hopf bifurcation (creation and merger) points. Our experiment finds more exciting dynamics in this parameter region. For damping values near $\alpha=0.05$, many complex nonplanar motions are found.

In the low-damping regime, persistent chaotic motions are observed over a wide range of forcing amplitudes and detunings. We observe both Lorenz and Rössler²² like chaos (see Fig. 12). Some typical parameters for which these motions are found are $\Delta t=1$ s, $f_0=1.3375$ kHz, $f=1.45$ kHz with

- $I_{\text{rms}}=34.7$ mA. Lorenz like chaos at $\alpha=0.090$, and
- $I_{\text{rms}}=31.5$ mA. Rössler like chaos at $\alpha=0.095$.

To plot these results we use the “differential-integral” embedding described by Gilmore and Lefranc.²² Specifically, if $x_1(i)$ is the sampled data, then this embedding is defined by $y_1(i)=x(i)+\exp(-1/\tau)x_1(i-1)$, $y_2(i)=x(i)$, and $y_3(i)=x(i)-x(i-1)$, where τ is chosen to cover several oscillations, but not long enough to show a systematic drift (varying mean value) in the embedded data.

If the forcing is increased the motion gets far more complicated with multiple, coexisting attractors—many of them chaotic. The motions of the string in this low-damping regime appear to mirror those of the string with a higher damping, modulated by a third, much lower, frequency.

V. CONCLUSION

We have examined the dynamics of a forced taut string and found good qualitative agreement with predictions from

the averaged equations of motion in the high damping regime. These equations are derived by truncating to the fundamental mode and averaging out the fast forcing time scale, but allow for motion in both transverse directions with implicit coupling via longitudinal motion. Quantitative agreement was not present since we found a systematic shift in the parameters required to observe bifurcations predicted by the averaged equation model. In addition we found a rich set of complex motions occurring at low damping and large detunings which do not appear to occur in the averaged model.

It is possible that the model could be improved by including a more realistic description of the damping. Air resistance and internal friction are not, contrary to the assumptions of the model, proportional to the velocity of the string over the entire decay envelope. Altering the damping model may yield a more comprehensive agreement with these experimental results. We should note, however, that Bajaj and Johnson⁵ also compared parameter values for various bifurcations in the the averaged equation model with the unaveraged string model and also found that bifurcation parameter values were shifted between these different models.

We have tried to make these data sets widely available via ftp download, and some of the data described in this paper have been investigated by other researchers exploring such topics as nonlinear noise reduction, chaotic synchronization, topological analysis of chaotic time series, and so on.^{21,22,32-40} There is still much to be learned from the sound of one string vibrating.

APPENDIX: STRING CONTROLLER AND PARAMETER CONVERSIONS

To collect data for the string experiment we need to sample the motion an integer number of times per forcing period. An appropriate sampling trigger can be generated with a phase locked loop (PLL), locking a high frequency square wave to a square wave of the same frequency as the forcing sine wave. Unfortunately, such PLL’s can be very difficult to design without phase drift.

Therefore we used a different approach. Instead of obtaining the sampling trigger from the forcing signal, the forcing signal is derived from a high frequency (≈ 100 kHz) square wave from which the sampling trigger is also derived. This has many advantages but poses several technical problems: Namely, producing a sine wave from a square wave keeping the amplitude of the sine wave independent of the frequency of the square wave. This is important since a common experimental procedure is to scan the forcing frequency while observing the resulting behavior. The solution lay in a filter module based on a National Semiconductor LMF60 CIN-50 sixth-order, switch-capacitor, Butterworth low-pass filter chip. This chip gives 36 dB per octave suppression above a critical frequency f_c which is determined by an external clock input divided by 50. If this external clock has frequency times the desired sine-wave output frequency then the cutoff frequency is 1.28 times the input square wave frequency. The filter then attenuates the n th harmonic component of the input square wave by a factor of $10^{-2.81n}$, and the deviation from sinusoidal of the output of the filter can be calculated by evaluating the filter function for the Fourier components of the input and summing these together. The filtered out function becomes $4/\pi(\cos(\omega t)-10^{8.9}\cos(3\omega t)+\dots)$. This gives a noise level (from filter imperfections) of less than $10^{-6}\%$.

Table I. Parameters of the string experiment. These are used to determine the formulas for conversion between experimental and numerical parameters.

Symbol	Quantity	Value
l	length	0.07 m
l_F	forcing length	0.045 m
m	mass per unit length	3.39×10^{-4} kg m $^{-1}$
ρ	density	2.1×10^4 kg m $^{-3}$
Y	Young's modulus	$197\,778 \times 10^6$ N m $^{-2}$
B	Magnetic field strength	0.2 ± 0.05 T
Δt	90%–10% decay time	0.1 s
f_0	free vibration frequency	1.385 kHz
I_{rms}	forcing current	20–600 mA

Signals from the strings are sampled and averaged in real time on a digital signal processor designed and constructed for the task at hand. The ADSP 2105 Digital Signal Processor (DSP), made by Analog Devices Ltd., is the main processing unit. It is a 16 bit device with a pipelined Harvard Architecture, a peak performance of 60 million operations/s, and an instruction set optimized for digital signal processing. The data are sampled at 16 bit resolution and average on the DSP computer over one cycle (32 samples) to produce p and q components. This averaged data are then transmitted to a host computer (Macintosh SE/30) via a small computer system interface port. A more detailed description of the hardware and software used in this experiment is given in Ref. 10 and the paper by Brundell and Molteno.²⁵

The parameters of the averaged equations of motion are dimensionless. In order to investigate phenomena in the parameter ranges examined by Bajaj and Johnson^{5,6} and to make a quantitative comparison to the theoretical models, we need to express these parameters as functions of easily altered experimental quantities. The parameters of interest are:

- f_0 , the frequency of free vibration (small amplitude) of the fundamental mode, controlled by adjusting the tension or length of the string;
- Δt , the 90%–10% decay time for the amplitude of the string once forcing is switched off. This determines the natural damping which is equal to the decay rate towards equilibrium behavior divided by $2\pi f_0$. Δt is controlled by the application of a silicone coating to the string as in O'Reilly and Holmes;⁷
- f , the frequency of excitation; and
- I_{rms} , the rms excitation current (a measure of the strength of the excitation).

The expressions relating the parameters used in the averaged equations of motion (α, β) to the experimental parameters shown in Table I are

$$\alpha = \frac{k_\alpha f_0}{\Delta t I_{\text{rms}}^{2/3}}, \quad \beta = \frac{k_\beta (f^2 - f_0^2)}{I_{\text{rms}}^{2/3}}. \quad (\text{A1})$$

The constants of proportionality, also in terms of the experimental parameters (see Table I) are given by

$$k_\alpha = \frac{4 \log 9 l^2 m}{(2B^2 Y l_f^2)^{1/3}}, \quad k_\beta = \frac{8 l^2 (\pi^2 m^2 \rho)^{1/3}}{(2B^2 Y l_f^2)^{1/3}}. \quad (\text{A2})$$

The parameter ranges investigated by Bajaj and Johnson were $\alpha \in [0.1, 1]$ and $\beta \in [0.5, 1]$. With $\Delta t = 0.1$ s, these theo-

retical parameters correspond to the experimental parameters in the range $I_{\text{rms}} \in [20 \text{ mA}, 600 \text{ mA}]$ and $f \in [f_0, f_0 + 80 \text{ Hz}]$.

The phenomenological damping inserted into the equations of motion implies an exponential decay towards the resting state of the string. In the experiment damping is more complex, and it does not depend linearly on the velocity over the entire decay envelope. However, as we are using a linear damping model, we take a linear fit of the logarithm of the decaying amplitude as the damping term used in the equations of motion. This linear fit to a nonlinear function could be the cause of some discrepancies between the model and experiment.

^aElectronic mail: nbt@alumni.reed.edu

¹J. B. Keller, "Large amplitude motion of a string," *Am. J. Phys.* **27**, 584–586 (1959).

²P. Morse, *Vibrations and Sound*, 2nd ed. (McGraw-Hill, Boston, MA, 1936).

³J. A. Elliott, "Intrinsic nonlinear effects in vibrating strings," *Am. J. Phys.* **48**, 478–480 (1980); "Nonlinear resonance in vibrating strings," *ibid.* **50**, 1148–1150 (1982).

⁴N. B. Tuffillaro, "Nonlinear and chaotic string vibrations," *Am. J. Phys.* **57**, 408–414 (1989).

⁵J. Johnson and A. Bajaj, "Amplitude modulated and chaotic dynamics in resonant motion of strings," *J. Sound Vib.* **128**, 87–107 (1989).

⁶A. Bajaj and J. Johnson, "On the amplitude dynamics and crisis in resonant motion of stretched strings," *Philos. Trans. R. Soc. London, Ser. A* **338**, 1–41 (1992).

⁷O. O'Reilly and P. Holmes, "Non-linear, non-planar and non-periodic vibrations of a string," *J. Sound Vib.* **153**, 413–435 (1992).

⁸O. O'Reilly, "Global bifurcations in the forced vibrations of a damped string," *Int. J. Non-Linear Mech.* **28**, 337–351 (1993).

⁹T. Molteno and N. Tuffillaro, "Torus doubling and chaotic string vibrations: Experimental results," *J. Sound Vib.* **137**, 327–330 (1990).

¹⁰T. C. A. Molteno, "Chaos and crisis in strings," Ph.D. thesis, University of Otago, Dunedin, New Zealand, 1994.

¹¹R. J. Hanson, J. M. Anderson, and H. K. Macomber, "Measurements of nonlinear effects in a driven vibrating-wire," *J. Acoust. Soc. Am.* **96**, 1549–1556 (1994).

¹²N. Tuffillaro, T. Abbott, and J. Reilly, *An Experimental Approach to Non-linear Dynamics and Chaos* (Addison-Wesley, Reading, MA, 1992).

¹³S. Strogatz, *Nonlinear Dynamics and Chaos* (Addison-Wesley, Reading, MA, 1994).

¹⁴R. C. Hilborn and N. B. Tuffillaro, "Resource letter: ND-1: nonlinear dynamics," *Am. J. Phys.* **65**, 822–834 (1997).

¹⁵J. E. Berger and G. Nunes, "A mechanical Duffing oscillator for undergraduate laboratory," *Am. J. Phys.* **65**, 841–846 (1997).

¹⁶B. K. Jones and G. Trefan, "The Duffing oscillator: A precise electronic analog chaos demonstrator for the undergraduate laboratory," *Am. J. Phys.* **69**, 464–469 (2001).

¹⁷N. Sungar, J. P. Sharpe, M. J. Moelter, N. Fleishon, K. Morrison, J. McDill, and R. Schoonover, "A laboratory-based nonlinear dynamics course for science and engineering students," *Am. J. Phys.* **69**, 591–597 (2001).

¹⁸R. Narasihma, "Non-linear vibration of an elastic string," *J. Sound Vib.* **8**, 134–146 (1968).

¹⁹J. Miles, "Resonant, nonplanar motion of a stretched string," *J. Acoust. Soc. Am.* **75**, 1505–1010 (1984).

²⁰J. Guckenheimer and P. Holmes, *Nonlinear Oscillations, Dynamical Systems, and Bifurcations of Vector Fields* (Springer-Verlag, New York, NY, 1983).

²¹K. Judd and A. Mees, "Modeling chaotic motions of a string from experimental data," *Physica D* **92**, 221–236 (1996).

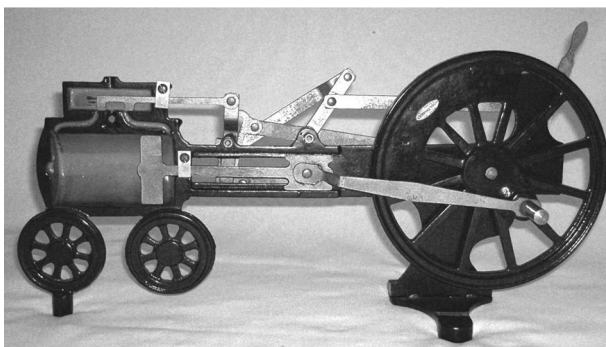
²²R. Gilmore and M. Lefranc, *The Topology of Chaos* (Wiley-Interscience, New York, NY, 2002).

²³C. Grebogi, E. Ott, and J. Yorke, "Crises, sudden changes in chaotic attractors and transient chaos," *Physica D* **7**, 181–200 (1983).

²⁴R. Hanson, "Optoelectronic detection of string vibration," *Phys. Teach.* (March 1987), 165–166.

²⁵J. Brundell and T. Molteno, *Radioscientist* **5**, 124 (1994).

- ²⁶D. M. Walker, N. B. Tufillaro, and P. Gross, "Radial-basis models for feedback systems with fading memory," *IEEE Trans. Circuits Syst., I: Fundam. Theory Appl.* **48**, 1147–1151 (2001).
- ²⁷L. Barford, N. Tufillaro, D. Usikov, L. Marochnik, and R. McCutcheon, "Calibration of Hubble space telescope focal-length variations using the emedding technique," *Flight Mechanics Symposium (NASA)*, edited by John P. Lynch, Goddard Space Flight Center, Greenbelt, Maryland, June 19–21 2001, pp. 485–495.
- ²⁸E. Knobloch and N. Weiss, "Bifurcations in a model of magnetoconvection," *Physica D* **9**, 379–407 (1983).
- ²⁹T. Molteno, "A fast $O(n)$ box-counting algorithm for estimating dimensions," *Phys. Rev. E* **48**, 3263–3266 (1993).
- ³⁰J. Miles, "Damped spherical pendulum," *J. Sound Vib.* **140**, 327–330 (1993).
- ³¹E. Ott, *Chaos in Dynamical Systems* (Cambridge University Press, Cambridge, U.K., 1993).
- ³²H. Kantz and T. Schreiber, *Nonlinear Time Series Analysis* (Cambridge University Press, Cambridge, U.K., 1997).
- ³³R. Brown, N. Rulkov, and N. Tufillaro, "Synchronization of chaotic systems—the effects of additive noise and drift in the dynamics of the driving," *Phys. Rev. E* **50**, 4488–4508 (1994).
- ³⁴N. B. Tufillaro, P. Wyckoff, R. Brown, T. Schreiber, and T. Molteno, "Topological time series analysis of a string experiment and its synchronized model," *Phys. Rev. E* **51**, 164–174 (1995).
- ³⁵D. M. Walker and A. Mees, "Reconstructing nonlinear dynamics by extended Kalman filtering," *Int. J. Bifurcation Chaos Appl. Sci. Eng.* **8**, 557–569 (1998).
- ³⁶R. Gilmore, "Topological analysis of chaotic systems," *Rev. Mod. Phys.* **70**, 1455–1529 (1998).
- ³⁷D. Allingham, M. West, and A. I. Mees, "Wavelet reconstruction of nonlinear dynamics," *Chaos* **8**, 2191–2201 (1998).
- ³⁸R. Hegger, H. Kantz, and T. Schreiber, "Practical implementation of nonlinear time series methods: The TISEAN package," *Chaos* **9**, 413–435 (1999).
- ³⁹K. Judd and M. Small, "Towards long-term prediction," *Physica D* **136**, 31–44 (2000).
- ⁴⁰M. Small, K. Judd, and A. Mees, "Modeling continuous processes from data," *Phys. Rev. E* **65**, 046704 (2002).



Steam Engine Half Model. Up to the middle of the 20th century, introductory textbooks had cutaway drawings of steam engines, and apparatus manufacturers responded with half-models showing the working parts. This model of a locomotive engine can be found in the 1925 Chicago Apparatus Company catalogue for \$6.00. This is a fairly big device, 38 cm long and 18 cm high. Shifting the reversing gear back and forth moves the slider in the steam box atop the cylinder so that the steam will be admitted first to the front or the back of the piston. The model is in the Greenslade Collection. (Photograph and notes by Thomas B. Greenslade, Jr., Kenyon College)